JOURNAL OF COMPUTATIONAL PHYSICS 94, 314–351 (1991)

Nonlinear Fourier Analysis for the Infinite-Interval Korteweg-de Vries Equation II: Numerical Tests of the Direct Scattering Transform

A. PROVENZALE AND A. R. OSBORNE

Istituto di Fisica Generale dell'Università and Istituto di Cosmo-Geofisica del C.N.R., Via Pietro Giuria 1, Torino 10125, Italy

Received June 6, 1989; November 14, 1989

A recursive algorithm for computing the direct scattering transform (DST) of a discrete space or time series whose dynamics is described approximately by the infinite-line Korteweg–de Vries (KdV) equation is tested for numerical accuracy by considering several example problems for which the exact DST spectrum is known. The effects of truncation, roundoff, discretization, and noise errors are specifically addressed. Procedures for estimating errors in a general experimental context are developed and the nonlinear filtering of noise is discussed. © 1991 Academic Press, Inc.

CONTENTS

1. INTRODUCTION

The Korteweg–de Vries (KdV) equation arises as a canonical model equation in a variety of physical problems [1]. In a fluid dynamical context the KdV equation on the infinite interval describes the evolution of one-dimensional, localized long waves in shallow water (a Cauchy problem): an initial wave pulse (Fig. 1a) evolves into solitons and dispersive radiation in the far field (Fig. 1c). In this paper we are primarily concerned with computing the nonlinear Fourier, temporally invariant

0021-9991/91 $3.00

Copyright © 1991 by Academic Press, Inc.
All rights of reproduction in any form reserved.

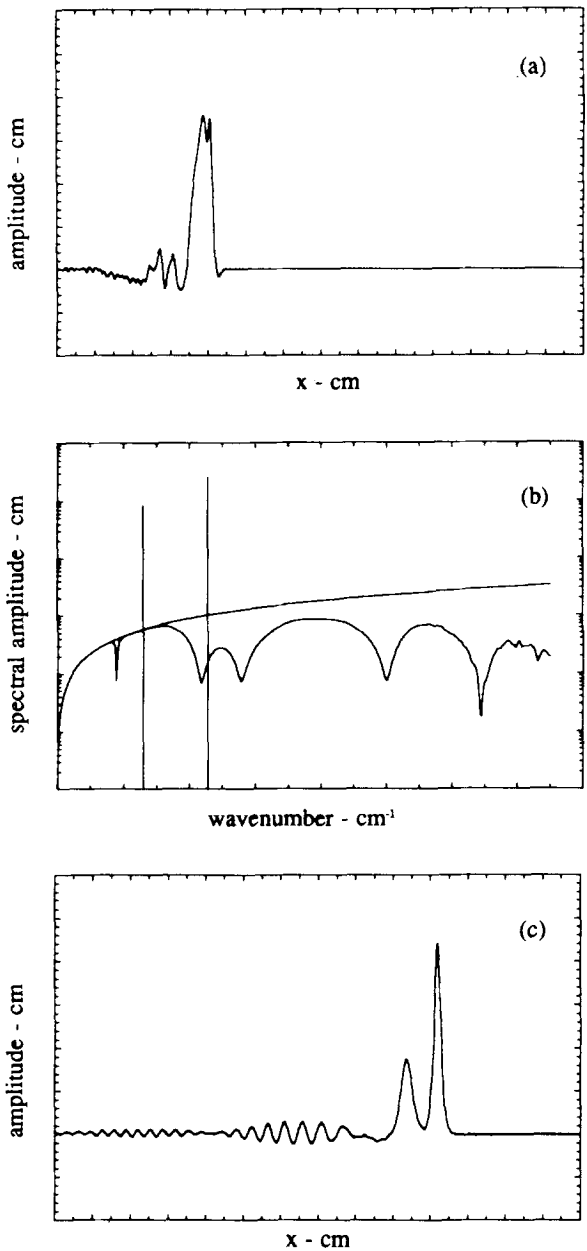

FIG. 1. An initial wave (depicted in (a)) evolves in the far field into solitons and a radiative tail (c). The DST spectrum of the initial wave, reported in (b), contains information about the far-field evolution of the initial wave. In this panel the upper solid curve represents a saturation spectrum and the intermediate solid curve is the DST continuous spectrum. The discrete soliton eigenvalues (two in this situation) are represented by solid vertical lines.

spectral amplitudes of this wave motion (Fig. 1b); in the spectrum the solitons are represented by the vertical lines and the radiation spectrum is the continuous curve. The nonlinear spectral solution to the Cauchy problem for the KdV equation on the infinite interval was found by Gardner, Greene, Kruskal, and Miura [2]. For a review and extension of these mathematical methods to other physically interesting problems see [1, 3–7]. A key feature of this approach is that it may be viewed as a generalization of Fourier transform theory and is normally referred to as the *inverse scattering* transform. In the companion paper ([8], hereinafter referred to as I) we review the spectral structure of this theory and derive a two-point recursive algorithm for computing the direct scattering transform (DST) of a localized wave field. The motivation for developing the DST algorithm is to provide a tool for probing the spectral structure of nonlinear experimental or computer generated data supplied in the form of space or time series.

One aim of the present paper is to apply the DST algorithm to a number of situations for which exact answers are known. The comparison between exact and numerical results allows for the validation of the numerical procedures. We explore the effects of truncation and roundoff errors on the spectrum; errors introduced by the discretization of the input wave form are also considered. We further consider procedures for applying the numerical DST to the analysis of data contaminated by random noise.

The DST algorithm was developed by analogy with the discrete, finite Fourier transform. The requisite nonlinear spectrum is a wavenumber representation of a wave field (as a function of space x) which is frozen at some arbitrary time t_0. Alternatively it may be viewed as a frequency domain representation of a wave field which varies as a function of time t and corresponds to some fixed spatial location x_0. Just as the Fourier transform is a wavenumber or frequency domain representation of some linear wave motion, the DST is a spectral representation of nonlinear wave motion described by the KdV equation. Like the Fourier transform the DST has the important property that the spectrum evolves simply in time: the spectral amplitudes are constants while the phases vary sinusoidally (continuous spectrum) or exponentially (soliton spectrum). Exploitation of this simple motion in an experimental and numerical context has provided a prime motivation for applying the DST approach as a kind of nonlinear Fourier analysis [9–16]. Several important features of the approach taken here are that the DST algorithm: (a) is relatively fast and allows for efficient machine analysis of space or time series of several thousands of points; (b) is rather general in that it may be applied to any space or time series which is governed approximately by the Kortweg–deVries equation; (c) has relatively high accuracy and allows for a rather precise determination of the nonlinear spectrum; and (d) allows for the nonlinear filtering of selected spectral components and of noise. Another important characteristic of the DST algorithm given herein is that it is easily extendable to the case of periodic boundary conditions [17, 18].

The remainder of this paper is organized as follows. In Section 2 we consider some of the possible physical applications of the DST approach and in Section 3

we discuss the implementation of the numerical algorithm for the DST. In Section 4 we consider cases for both positive and negative square wave pulses, whose spectra are known analytically (see I); these serve as controls for the numerical checkout of the DST algorithm and provide information about truncation and roundoff errors. A comparison between the DST spectrum and the linear Fourier spectrum is also considered. In Section 5 we compare the DST algorithm with the N-soliton solution of the KdV equation. Even though no continuous spectrum is theoretically present in this case, the discretization procedure used herein, and its associated numerical algorithm, compute some finite (albeit small) value for the continuous spectrum. Thus this series of tests provides a measure of numerical uncertainties in the continuous spectrum; we provide procedures for estimating these discretization errors. In Section 6 we consider cases where random errors are superposed on theoretically known input wave forms. This provides a basis for estimating the effects of noise error on the DST spectrum for certain types of experimental data. Procedures for the removal of noise from data by nonlinear filtering are also considered. A summary and conclusions are provided in Section 7.

2. Spectral Analysis of Space and Time Series

We consider here the case of unidirectional, weakly nonlinear waves in shallow water in 1 (space) + 1 (time) dimensions for which the canonical governing partial differential equation (PDE) is the Korteweg–de Vries equation (see (2.1) and further discussion below) whose field is the wave amplitude $\eta(x, t)$. The time evolution of wave motion of this type may be thought of in terms of a *Cauchy problem*: given the state of the system at some time t_0, $\eta(x, t_0)$, determine the motion at some future (or past) time t, $\eta(x, t)$. Alternatively, one may seek to solve the related *boundary value problem*: given the temporal evolution of some system at a fixed spatial location x_0, $\eta(x_0, t)$, determine the behavior of the motion at some other spatial location x, $\eta(x, t)$. This latter problem is not solvable by the conventional form of the KdV equation. Both of these kinds of descriptions are said to be Eulerian: the dynamical variable of interest ($\eta(x, t)$) is a function of the independent variables space x and time t. In experiments one normally measures (1) time series of the wave motion at a selected fixed spatial location, $\eta(x_0, t)$, or (2) space series at a fixed time, $\eta(x, t_0)$.

The dimensional form of the conventional or "space" Eulerian KdV equation is given by

$$\eta_t + c_0\eta_x + \alpha\eta\eta_x + \beta\eta_{xxx} = 0, \tag{2.1}$$

where c_0, α, β are real constants. For surface water waves $c_0 = (gh)^{1/2}$, $\alpha = 3c_0/2h$, and $\beta = c_0h^2/6$, h is the water depth, g is the acceleration of gravity. An important quantity in the following analysis is also $\lambda = \alpha/6\beta$ or equivalently, for water waves, $\lambda = 3/2h^3$. Other fluid mechanical applications of the KdV equation have been

found for internal wave motions [19] and for geophysical fluid dynamical (GFD) motions [6, 20–24]. The KdV equation (2.1) is normally derived from the Euler equations with a (singular) perturbation expansion in powers of the nonlinearity parameter $\varepsilon = |\eta_0/h|$ and of the dispersion parameter $\delta^2 = (h/L)^2$, where η_0 is a typical wave amplitude and L is a typical wavelength. The KdV equation is obtained by assuming $\varepsilon \ll 1$, $\delta^2 \ll 1$, where $\varepsilon \approx \delta^2$; KdV is accurate to order ε (i.e., to first order in nonlinearity). Equation (2.1) solves the Cauchy problem: the time evolution $\eta(x, t)$ of a localized initial wave $\eta(x, 0)$ is determined by (2.1) for all $t > 0$ such that $-\infty < x < \infty$. We may also determine the (nonlinear) Fourier spectrum (scattering transform) of the initial wave $\eta(x, 0)$ by the methods discussed here and in paper I.

From an experimental point of view, however, one normally measures $\eta(0, t)$; given this single time series, Eq. (2.1) is not a well-posed problem and the spatial evolution of the wave $\eta(x, t)$ cannot be found purely from the space KdV equation, nor can spectral analysis of the time series $\eta(0, t)$ be conducted. In order to confront this difficulty we consider an alternate form of the KdV equation proposed by Karpman [25] and Ablowitz and Segur [1] (see also Osborne *et al.* [26]). This is given by

$$\eta_x + c_0' \eta_t + \alpha' \eta \eta_t + \beta' \eta_{ttt} = 0, \tag{2.2}$$

where

$$c_0' = 1/c_0; \qquad \alpha' = \alpha/c_0^2; \qquad \beta' = -\beta/c_0^4. \tag{2.3}$$

We refer to Eq. (2.2) as the "time" KdV equation (because of the time derivatives in the dispersive term); this equation is well defined as a boundary value problem, so that given $\eta(0, t)$, then (2.2) evolves the wave over all space $\eta(x, t)$. Segur [1, 27] has given a rigorous derivation of (2.2) using the singular perturbative approach (see also Newell [28], Osborne *et al.* [26, 29]); (2.1) and (2.2) are both accurate to first order in ε and δ^2 and, based upon singular perturbation theory, there is no way to state which of these equations may be preferable to the other. It remains for experiments to decide whether one equation is preferable to the other for large ε.

Note that (2.2) has the form of the KdV equation except that the roles of space x and time t have been reversed and the constant coefficients have been changed. This reversal of the emphasis on space and time means that the direct scattering transform algorithm may be used to analyze *both* space and time series. For space series one of course obtains a wavenumber spectrum as discussed at length in I. For the analysis of time series it is easy to show that a simple change of variable is required in going from the spectral problem for (2.1) to that for (2.2):

$$\lambda \to c_0^2 \lambda, \qquad K_n \to \Omega_n; \qquad k \to \omega; \qquad x \to t. \tag{2.4}$$

This implies that a DST analysis of a time series may be conducted by reinterpreting: (1) the wavenumber as frequency, (2) space as time, and (3) rescaling the

parameter λ by c_0^2. The spectral domain now is in terms of the discrete and continuous frequencies Ω_n, ω, rather than in terms of wavenumbers K_n, k.

Finally, we recall that a different approach to the description of wave motion is based on the use of Lagrangian coordinates: in this case the emphasis is on following the individual particles in the fluid. Dynamically one seeks to determine the particle position $\mathbf{X}(\mathbf{a}, t)$ as a function of the reference position $\mathbf{a}$ of the particle and time t. The reference position $\mathbf{a}$ is generally considered to be the rest position of the particle for, say, $t \to -\infty$. For unidirectional water waves the motion is in vertical planes perpendicular to the wave crests, thus $\mathbf{X} = (X, Y)$ and $\mathbf{a} = (a, b)$, where X and a refer to the horizontal motions, while Y and b refer to the vertical motions. One thus obtains a set of partial differential equations for $X(a, b, t)$ and $Y(a, b, t)$, where now the particle positions $\mathbf{X}$ are the dynamical variables and their reference positions $\mathbf{a}$ and the time t are the independent variables. The *Cauchy problem* for the Lagrangian description is thus: given all the particle positions $\mathbf{X}(\mathbf{a}, t_0)$ at time t_0, for all possible values of the reference position $\mathbf{a}$, determine the positions $\mathbf{X}(\mathbf{a}, t)$ of all the particles at some future (or past) time t. The analogous related *boundary value problem* is: given the temporal evolution of some particle whose reference position is the particular value $\mathbf{a}_0$, $\mathbf{X}(\mathbf{a}_0, t)$, determine the motion of all the particles for all possible values of reference position $\mathbf{a}$, $\mathbf{X}(\mathbf{a}, t)$. An important result in the context of Lagrangian coordinates is that the particle orbits for shallow-water, weakly nonlinear wave motions at the KdV order of approximation are described by partial differential equations which have the same functional form as the Eulerian KdV equation, see [26]. Thus, the nonlinear spectral approach discussed in this paper may be immediately applied also to the case of Lagrangian coordinates.

3. Implementation of the Algorithm

We seek to implement the algorithm for the direct scattering transform of a discrete wave form described by a discrete space series of M values of the wave amplitude separated by some (presumed small) value of spatial interval Δx, $\{\eta_m = \eta(x_m, t_0);\ x_m = x_0 + m\Delta x,\ m = 1, M\}$. The equivalent problem on the time domain is obtained by substituting the scaling (2.4). As discussed in I we take the first two and last two points in $\{\eta_m\}$ to be zero. We now briefly discuss the recursive procedure for determination of the DST spectrum of this array of points. The nonlinear DST spectrum for the KdV equation in the space domain is given by

$$\text{DST} = \{K_n, C_n, N; b(k)\}, \tag{3.1}$$

where the K_n and C_n are the wavenumbers and phase coefficients of the N solitons and $b(k)$ is the continuous spectrum. For finite $b(k)$ and $N = 0$ the spectrum contains only radiation; for N finite and $b(k) = 0$ the spectrum contains only solitons. Further details are given in I.

To compute (3.1), given $\{\eta_m\}$, we first compute the spectral matrix $\mathbf{M}(\kappa)$ by:

$$\mathbf{M} = \mathbf{B}\mathbf{M}'\mathbf{A}, \tag{3.2}$$

where

$$\mathbf{B} = \begin{bmatrix} e^{-i\kappa(x_0 + \Delta x/2)} & 0 \\ 0 & e^{i\kappa(x_0 + \Delta x/2)} \end{bmatrix} \tag{3.3}$$

and

$$\mathbf{A} = \begin{bmatrix} e^{i\kappa(x_M - \Delta x/2)} & 0 \\ 0 & e^{-i\kappa(x_M - \Delta x/2)} \end{bmatrix}. \tag{3.4}$$

The matrix $\mathbf{M}'$ is given by

$$\mathbf{M}' = \prod_{m=1}^{M-1} \Delta\mathbf{T}_m, \tag{3.5}$$

where the "delta $\mathbf{T}_m$" matrix is a function of the discretization interval Δx and not of x_m. We write the matrix $\Delta\mathbf{T}_m$ in a form suitable for recursive computation

$$\Delta\mathbf{T}_m = \begin{bmatrix} s_m z^{-\zeta_m} & d_m z^{-\zeta_m} \\ d_m z^{\zeta_m} & s_m z^{\zeta_m} \end{bmatrix}, \tag{3.6}$$

where

$$\zeta_m = \{\lambda\eta(x_m, 0) + \kappa^2\}^{1/2} \tag{3.7}$$

$$z = e^{i\Delta x} \tag{3.8}$$

$$d_m = \frac{(\zeta_m - \zeta_{m+1})}{2\zeta_m} \tag{3.9}$$

$$s_m = \frac{(\zeta_m + \zeta_{m+1})}{2\zeta_m}. \tag{3.10}$$

The matrix $\mathbf{M}'$ may then be written as

$$\mathbf{M}' = \prod_{m=1}^{M-1} \Delta\mathbf{T}_m = \begin{bmatrix} z^{-\rho_{M-1}} F_{M-1}(z) & z^{-\rho_{M-1}} G_{M-1}(z) \\ z^{\rho_{M-1}} G_{M-1}(1/z) & z^{\rho_{M-1}} F_{M-1}(1/z) \end{bmatrix}, \tag{3.11}$$

such that $F_m(z)$ and $G_m(z)$ satisfy the recursion relations

$$\begin{bmatrix} F_m(z) \\ G_m(z) \end{bmatrix} = \begin{bmatrix} s_m & d_m z^{2\zeta_m} \\ d_m & s_m z^{2\zeta_m} \end{bmatrix} \begin{bmatrix} F_{m-1}(z) \\ G_{m-1}(z) \end{bmatrix} \tag{3.12}$$

with

$$F_0(z) = 1, \qquad G_0(z) = 0 \tag{3.13}$$

and

$$\rho_{M-1} = \frac{1}{2} \sum_{m=1}^{M-1} \zeta_m. \tag{3.14}$$

Recursion formulas (3.12)–(3.14) for the direct scattering transform are analogous to the recursion formula (5.6) given in I for the Fourier transform. Execution of (3.12) requires M^2 operations as one iterates over space x and wavenumber κ. It is worth pointing out that the recursion relations for $[F_m(z), G_m(z)]$ and $[F_m(1/z), G_m(1/z)]$ do not functionally depend on one another. Since we need only matrix elements M_{11} and M_{12} to compute the DST and since by (3.11) we need only $F_{M-1}(z)$ and $G_{M-1}(z)$, then to calculate the infinite-line DST spectrum it is not necessary to compute the $[F_{M-1}(1/z), G_{M-1}(1/z)]$. This reduces the computational time by an additional factor of two.

Note that the spectral matrix is a function of the input wavenumber κ, which can be either pure imaginary ($\kappa = iK_n$), when searching for the soliton part of the spectrum, or real ($\kappa = k/2$), when computing the continuous spectrum. The continuous spectrum is computed from the simple formula

$$b(k) = -M_{12}(k/2)/M_{11}(k/2). \tag{3.15}$$

The discrete spectrum is determined from the zeros of M_{11}:

$$M_{11}(iK_n) = 0, \tag{3.16}$$

where the phase coefficients are found by

$$C_n^2 = \lim_{K \to K_n} (K - K_n)\, b(iK). \tag{3.17}$$

The number of solitons is computed from the transmission coefficient $a(k)$,

$$N = \lim_{k \to \infty} [\arg(a(k)) - \arg(a(-k))]. \tag{3.18}$$

To compute the radiation spectrum (3.15) one needs to determine both an upper limit and a resolution for the wavenumber. Since the spectrum is theoretically continuous we can make the resolution as small as we choose. However, for convenience we have elected to use a wavenumber cutoff and resolution consistent with periodic Fourier theory. Thus we use the Nyquist cutoff given by

$$k_N = \pi/\Delta x \tag{3.19}$$

and a spectral resolution

$$\Delta k = 2k_N/M. \tag{3.20}$$

A flow chart of the major features of the program is shown in Fig. 2 and details of the continuous and discrete spectral calculations are given in Fig. 3. We compute the continuous spectrum first (flow chart CONDST in Fig. 3a). The program flow chart is built around the call to the subroutine called MMAT which computes the spectral matrix by Eq. (3.2)–(3.14).

The flow chart for the discrete spectrum is shown in Fig. 3b. Here the wavenumber range extends to the maximum possible theoretical value given by

$$K_{\max} = (\lambda \eta_{\max})^{1/2}. \tag{3.21}$$

Note that imaginary wavenumber $\kappa = iK$ is iterated in the range $(0, K_{\max})$ and the subroutine MMAT is called on each iteration. If there is a sign change in the matrix element $M_{11}(iK)$ then the subroutine NEWTON is called to refine the estimate of the eigenvalue which is labeled K_n. NEWTON also computes the phase coefficients C_n by (3.17) after the search for the eigenvalue is complete. Note that the DST algorithm uses computer time proportional to M^2; thus doubling the number of points M increases the computer time by about a factor of four.

4. Investigation of Roundoff Errors

In this section we consider the application of the DST algorithm to an initial square wave pulse centered on the origin. For this particular problem the exact spectral solution of the scattering transform is known (see I) and it is thus possible to estimate the truncation and roundoff errors of the associated DST spectrum. We also use the case for a square input wave form to introduce a graphical representation and interpretation of the DST spectrum. In the following: (a) we compare the DST with the linear Fourier spectrum of the same wave in order to clarify some of the principal physical differences between linear and nonlinear Fourier analysis; (b) we compare the numerical DST with the exact analytical solution; and (c) we consider the effects of truncation errors in the input wave form. For the calculation of the DST and Fourier spectra discussed in this paper we used a vector processor FPS 164 (with 64-bit precision) attached to a host computer Digital VAX/750.

4.A. *Negative and Positive Square Waves–Comparison between the DST Spectrum and the Linear Fourier Spectrum*

We consider here a comparison between the DST and the linear Fourier transform for both negative and positive square waves. We first consider negative square waves with fixed half-length 100 cm (the square wave lies in the interval $-100\text{ cm} \leqslant x \leqslant 100\text{ cm}$ with amplitudes $\eta_0 = -0.1$ cm, -0.5 cm, -1.0 cm, and -4.0 cm). The water depth is fixed to be $h = 10$ cm and thus the nonlinearity parameter $\varepsilon = |\eta_0/h|$ varies from $\varepsilon = 10^{-2}$ to $\varepsilon = 0.4$. Here and in the following the input square wave form is placed on the interval $-250\text{ cm} \leqslant x \leqslant 250\text{ cm}$ and thus $L = 500$ cm. The DST spectra for these waves are reported in Fig. 4a–d. In the case of a negative square wave the soliton spectrum is absent and only the continuous

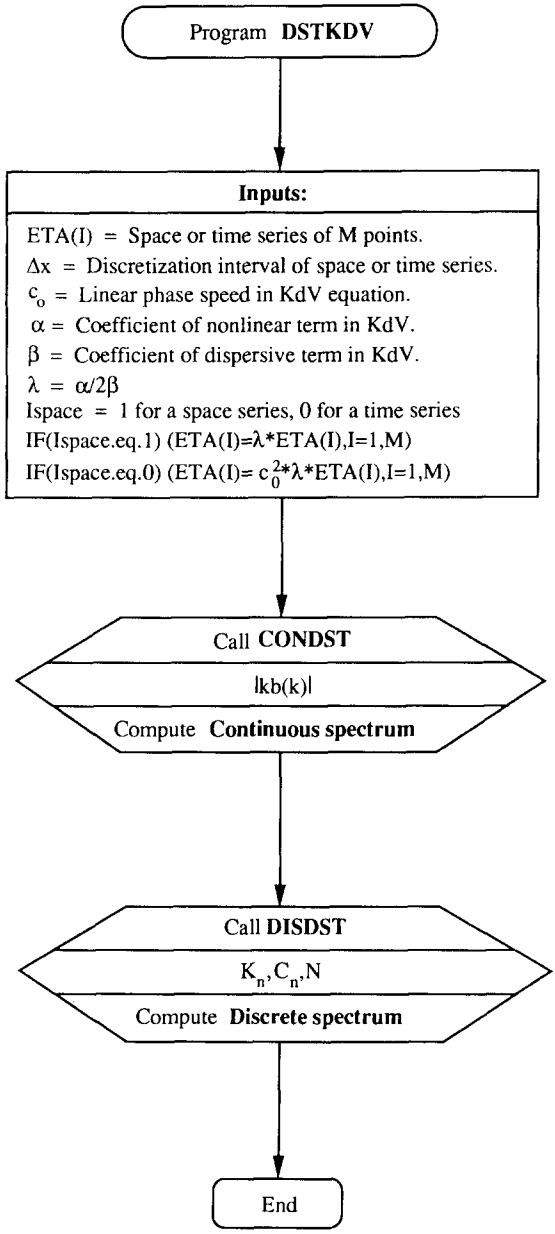

FIG. 2. Flow chart of the numerical DST algorithm.

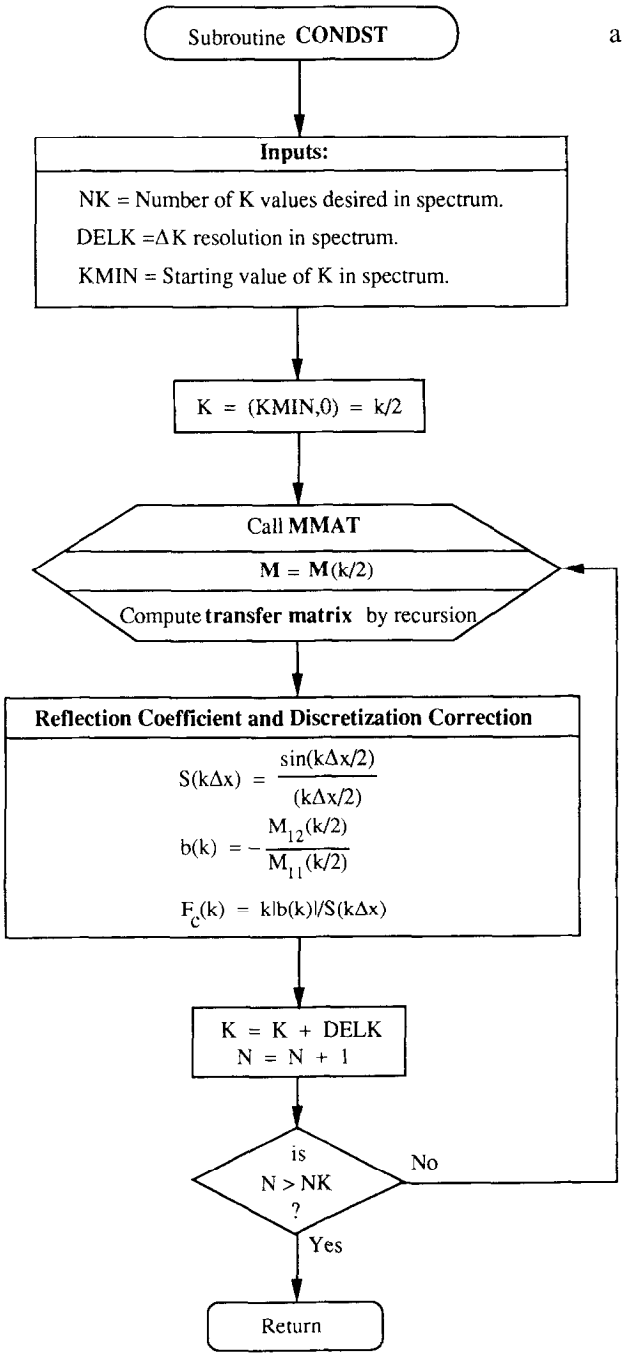

FIG. 3. Flow chart for the numerical calculation of the continuous DST spectrum (a) and of the discrete (soliton) spectrum (b).

b

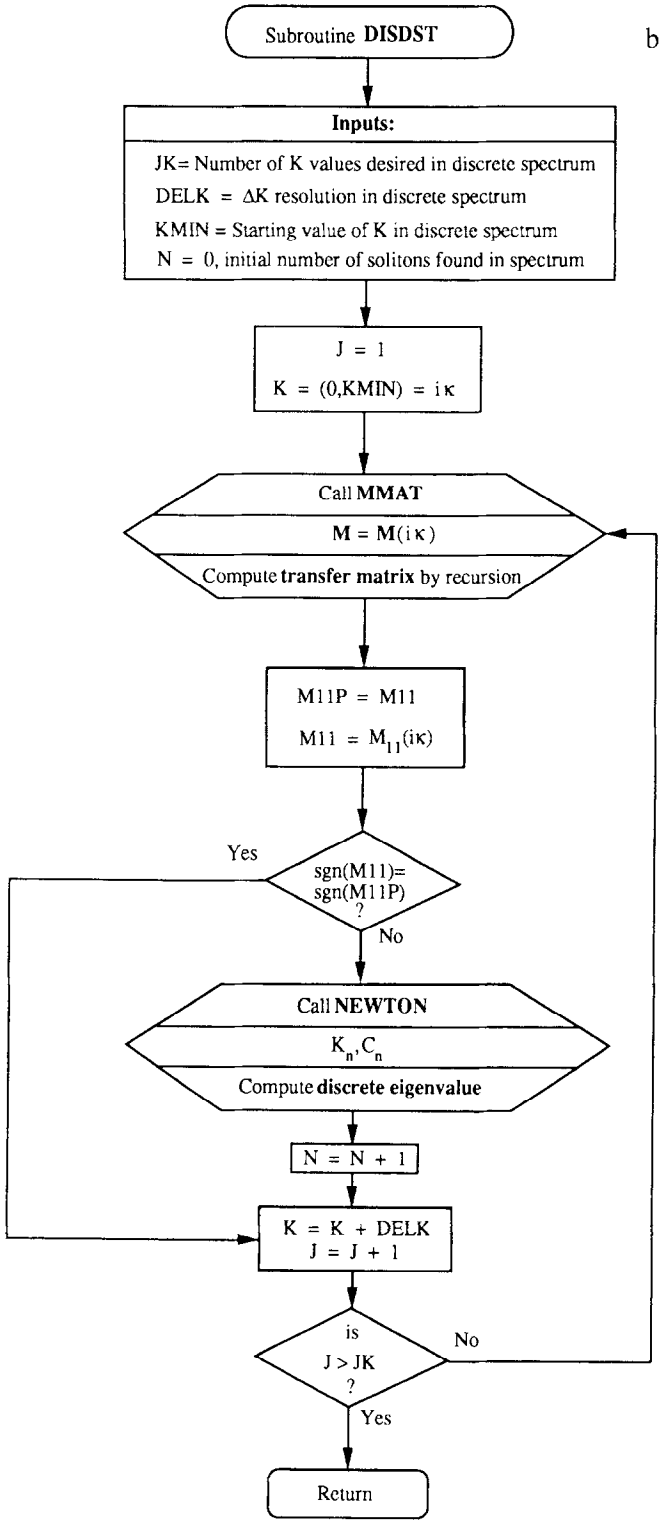

FIG. 3—*Continued*

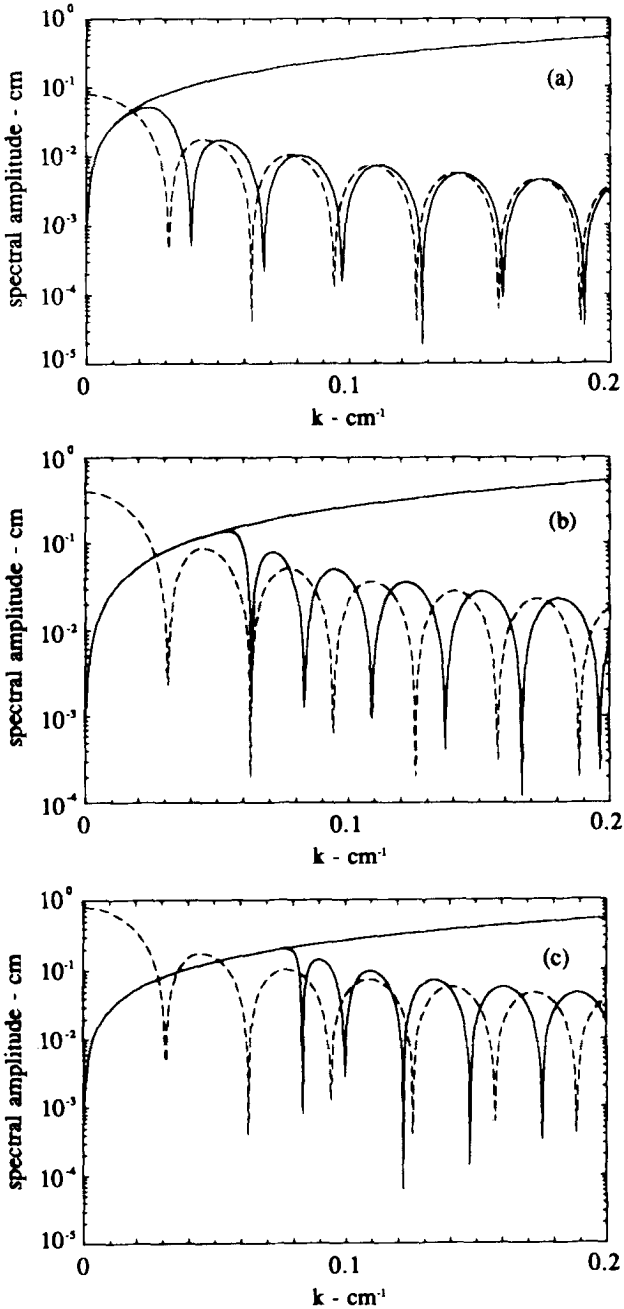

FIG. 4. DST spectra for a negative square wave with fixed half-length 100 cm and varying amplitude $\eta_0 = -0.1$ cm (a), $\eta_0 = -0.5$ cm (b), $\eta_0 = -1.0$ cm (c), and $\eta_0 = -4.0$ cm (d). No discrete spectrum is present for negative square waves. The upper solid curve represents a saturation spectrum, the intermediate solid curve is the DST continuous spectrum, and the dashed curve is the Fourier spectrum.

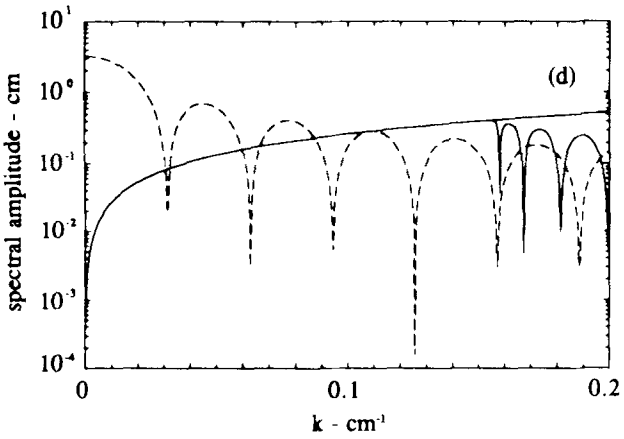

FIG. 4—*Continued*

spectrum is excited. In Fig. 4 the DST spectrum is represented by a solid line and the Fourier spectrum by a dashed line; we have graphed the spectral amplitudes, but not the phases. The continuous DST spectrum is graphed as

$$s(k) = k\,|b(k)|/\lambda L, \tag{4.1}$$

to be consistent with the periodic KdV spectrum (Osborne and Bergamasco [17, 18]). This normalization by λL allows direct comparison between the soliton amplitudes and the "radiative amplitudes" of the continuous spectrum; these latter may be viewed as spectral components which, through the Gelfand–Levitan–Marchenko equation (see I), nonlinearly superpose to give the radiative solution one observes in space-time. The upper solid line in Fig. 4 is a saturation curve which corresponds to the reflection coefficient $|b(k)| = 1$. The continuous DST spectrum cannot exceed this value, since $b(k)$ is constrained by the requirement $|b(k)| \leqslant 1$. For the linear Fourier spectrum $F(k)$ we have graphed $|F(k)|/\lambda L$; this normalization allows direct comparison with the continuous DST spectrum.

From Fig. 4 one sees that for very small amplitudes the continuous DST spectrum and the Fourier spectrum are quite similar. At large amplitudes, however, the differences are more and more pronounced due to stronger nonlinear interactions. Comparing the linear Fourier spectrum and the DST spectrum for negative square waves of moderate amplitude we find that (1) substantial differences occur at low wavenumbers (where there is the possibility of a saturation in the DST spectrum) and (2) at high wavenumbers where the linear and nonlinear spectra are often quite similar, but with the spectral lobes wavenumber-shifted relative to one another.

In Fig. 5a–d we show the DST spectra obtained for *positive* square waves with half-length 100 cm and amplitudes, respectively $\eta_0 = 0.1$ cm, $\eta_0 = 0.5$ cm, $\eta_0 = 1.0$ cm, and $\eta_0 = 4.0$ cm. The DST spectra now possess both a continuous and a discrete part. The discrete spectrum is represented by the vertical lines in Fig. 5. Each vertical

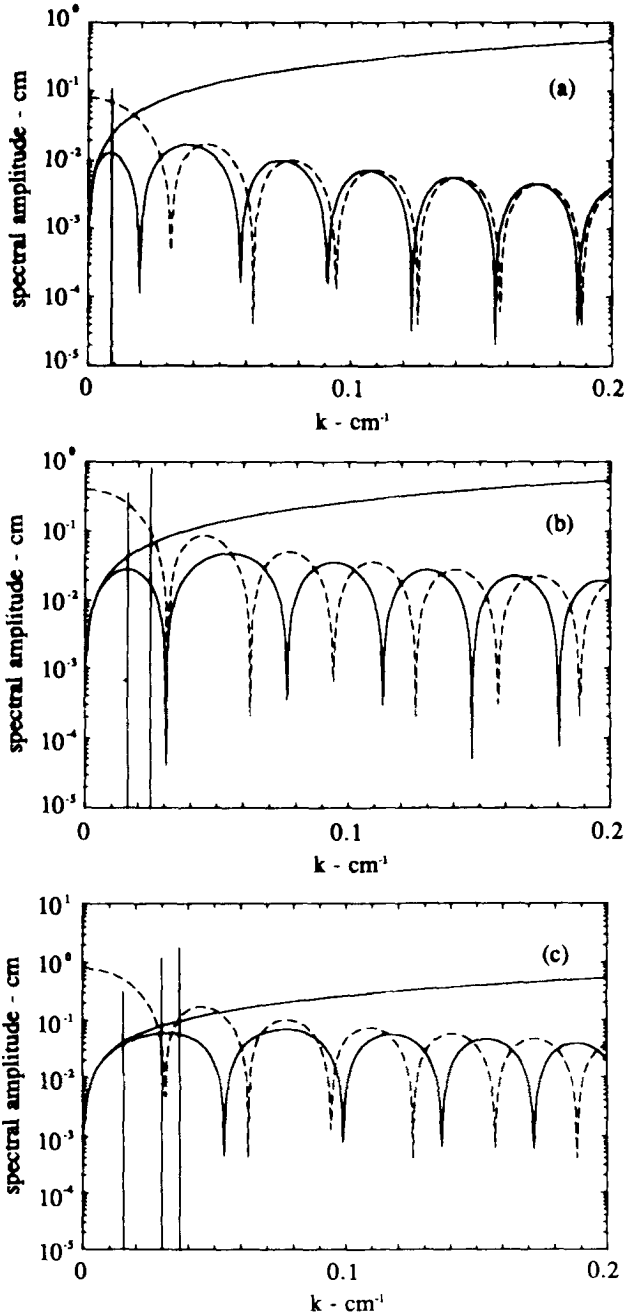

FIG. 5. DST spectra for a positive square wave with fixed half-length 100 cm and varying amplitude $\eta_0 = 0.1$ cm (a), $\eta_0 = 0.5$ cm (b), $\eta_0 = 1.0$ cm (c), and $\eta_0 = 4.0$ cm (d). The upper solid curve represents a saturation spectrum, the intermediate solid curve is the DST continuous spectrum and the dashed curve is the Fourier spectrum. The solid vertical lines represent the discrete soliton eigenvalues.

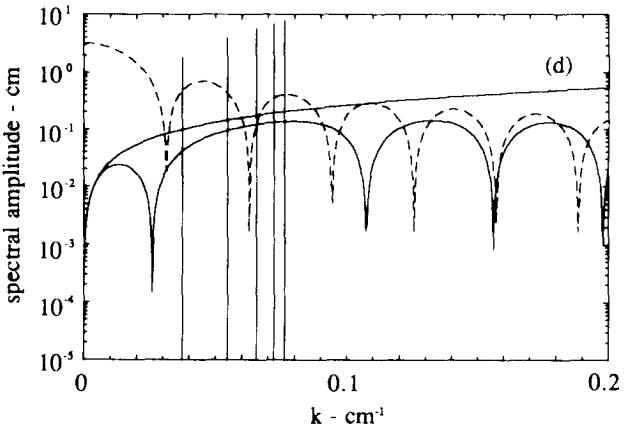

FIG. 5—*Continued*

line is the spectral representation of a soliton; the horizontal position of the line is determined by the wavenumber K_n of the soliton and its height by the soliton amplitude η_n. Since for the KdV equation the amplitude and the wavenumber of a soliton are related by $\eta_n = (2K_n^2/\lambda)^{1/2}$, it is clear that once the horizontal position of an arrow is given (i.e., the wavenumber) also its height is fixed. In this graphical representation we discard the phase information of the discrete eigenvalues, as we have also done for the continuous spectrum. In the present numerical experiment the number and the amplitude of the discrete eigenvalues (i.e., the solitons) increase with increasing initial amplitude η_0 of the positive square wave. Another effect is that for large wave amplitudes the continuous DST spectrum shows a tendency toward saturation ($|b(k)| = 1$) at low wavenumbers. We also observe that the continuous DST spectrum of the positive square wave forms is always smaller than the continuous spectrum of the corresponding negative waves (i.e., of square waves with amplitude $-\eta_0$ and equal half-length). This behavior, which is to be contrasted with the symmetry of the Fourier spectrum $|F(k)|$ with respect to the change $\eta_0 \to -\eta_0$, is due to the fact that for positive square waves a large portion of the energy is contained in the soliton (discrete) spectrum, and thus the energy content of the continuous DST spectrum is correspondingly depleted. For negative square waves no discrete spectrum is present and all the energy is contained in the continuous spectrum. This fact is a consequence of the well-known lack of symmetry of the KdV equation for changes of the kind $\eta(x, t) \to -\eta(x, t)$.

In Fig. 6a–c we show the DST and linear Fourier spectra for three positive square waves with fixed amplitude $\eta_0 = 1$ cm ($\varepsilon = 0.1$) for differing half-lengths 20 cm, 50 cm, and 200 cm, respectively ($\delta^2 = 0.0625$, 0.01, and 0.000625, respectively). The number of solitons and the tendency to saturation of the continuous spectrum increases with increasing values of the half-length. Due to the large wave amplitude chosen, differences between the linear and nonlinear spectra can be seen for all values of the half-length.

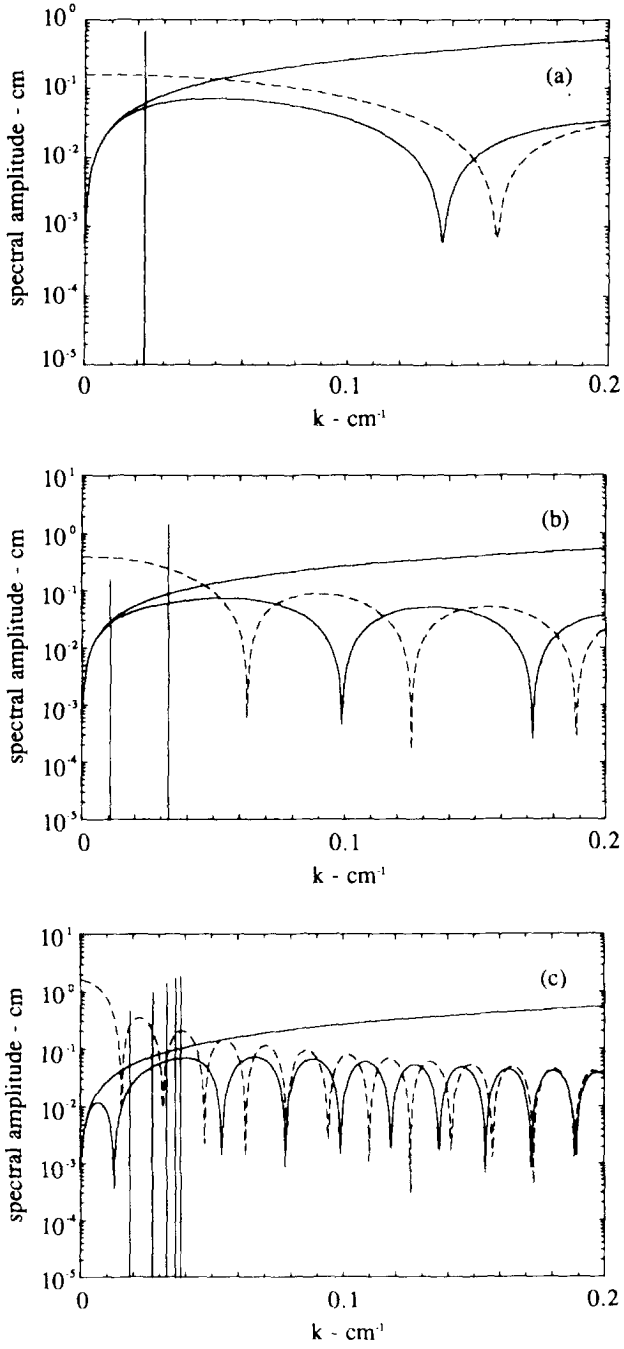

FIG. 6. DST spectra for positive square waves with fixed amplitude $\eta_0 = 1$ cm and varying half-length 20 cm (a), 50 cm (b), and 200 cm (c). Same details as in Fig. 5.

4.B. *Negative and Positive Square Waves—Comparison with the Exact Solution*

The DST spectrum for an initial square wave may be computed exactly by requiring the continuity of the Schroedinger wave function and of its first derivative at the right and left discontinuities of the wave (see I). To compare the numerical DST spectrum with the exact formulae we have chosen the same groups of examples already discussed above. Because the input wave form is exactly a square wave no discretization error is present in these cases, thus the roundoff errors inherent in the DST algorithm may be evaluated in detail. In all these examples we have found the DST algorithm to be quite precise and the results are practically indistinguishable from the exact values. Roundoff errors occur in the recursive calculation of the $\mathbf{M}(\kappa)$ matrix, where $4N$ multiplications are required to compute (3.11), (3.12) for a selected wavenumber. This implies that for typical space series of $N \approx 10^4$ points one loses about two decimals of accuracy in the elements of the $\mathbf{M}(\kappa)$ matrix, a fact we have verified by comparison of the analytical solution for the DST of a square wave to the numerical DST algorithm. Using double precision arithmetic implies an accuracy of 13 or 14 decimal digits for the elements of the $\mathbf{M}(\kappa)$ matrix.

4.C. *The Effects of Input Precision on the DST Spectrum*

We now briefly explore the effects of changing the precision of the input wave form and discuss how the DST spectrum is sensitive to these changes. We consider a square wave with half-length 100 cm and $\eta_0 = 4/3$ cm on a water depth $h = 10$ cm. In this case a low input precision implies a truncation of the wave amplitude and we expect to observe some differences in the DST spectra. Figure 7 reports the spectra obtained for an input precision of 16 significant figures (solid line) and of two significant figures (dashed line). There are visible differences between the two

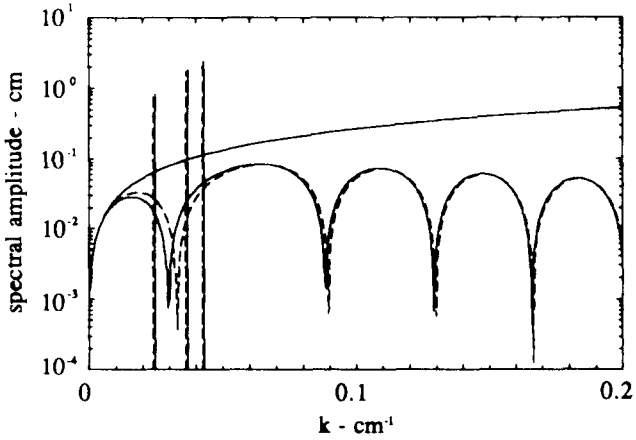

FIG. 7. DST spectra for a positive square wave with half-length 100 cm, and amplitude $\eta_0 = \frac{4}{3}$ cm for varying input precision. The solid line is for an input precision of 16 significant digits and the dashed line is for an input precision of two significant digits.

TABLE I

Relative Difference between the Exact and Numerically Computed Discrete (Soliton) Eigenvalues for Different Input Precison in the DST Algorithm for a Positive Square Wave

Number of significant figures	$\Delta\eta_1/\eta_1$	$\Delta\eta_2/\eta_1$	$\Delta\eta_3/\eta_3$
1	6.1×10^{-1}	3.4×10^{-1}	2.7×10^{-1}
2	6.5×10^{-2}	3.4×10^{-2}	2.7×10^{-2}
3	6.5×10^{-3}	3.4×10^{-3}	2.7×10^{-3}
4	6.5×10^{-4}	3.4×10^{-4}	2.7×10^{-4}
5	6.5×10^{-5}	3.4×10^{-5}	2.7×10^{-5}
6	6.5×10^{-6}	3.4×10^{-6}	2.7×10^{-6}
7	6.5×10^{-7}	3.9×10^{-7}	2.5×10^{-7}
8	6.1×10^{-8}	5.5×10^{-8}	$< 10^{-10}$
9	1.2×10^{-8}	$< 10^{-10}$	$< 10^{-10}$
10	$< 10^{-10}$	$< 10^{-10}$	$< 10^{-10}$

Note. Amplitude $\eta_0 = \frac{4}{3}$ cm and half-length 100 cm.

spectra which are generated by the fact that one spectrum corresponds to an amplitude $\eta_0 = 1.333333333333333$ and the other to $\eta_0 = 1.3$. Table I reports the amplitudes of the three solitons found for several values of the input precision. The results reported in Table I indicate that the errors in the soliton amplitudes are always of the same order of magnitude as the errors on the input wave form. This implies the important result that the truncation errors on the input wave are not amplified by the DST algorithm. The precision of the input wave form is essentially reflected in the spectral amplitudes found by the DST algorithm.

5. Investigation of Discretization Errors

In this Section we analyze the results of the DST algorithm for the pure N-soliton solutions of the KdV equation. This particular class of solutions is given by an exact expression which is discussed in the Appendix. Theoretically speaking, the DST spectrum of a pure N-soliton wave form is composed of N discrete eigenvalues, while the continuous spectrum is identically zero. Here we generate an N-soliton solution to the KdV equation and compute the nonlinear spectrum using the DST algorithm; the results are compared directly to the theoretical DST spectrum for the N-soliton solution. The numerical DST spectrum will differ in general from the exact spectrum mainly because of discretization errors (the truncation and roundoff errors have already been shown to be rather small). The principal consequence of discretization errors is the generation of a spurious continuous spectrum. We explore how these computational errors affect the DST spectrum and how the errors themselves are modified by changing the discretization step size.

As discussed in I the wave amplitude function $\eta(x, 0)$ is discretized into M points; then a piecewise constant wave form is associated with the discrete input as shown

in Fig. 1 of I. The DST algorithm furnishes the exact nonlinear spectrum of the piecewise constant wave form, which approaches the spectrum of the continuous wave amplitude function as $M \to \infty$ and the discretization step $\Delta x \to 0$. In what follows, "discretization error" will include not only the effect of discretizing the wave amplitude function $\eta(x, 0)$ but also the effect of replacing it with a piecewise constant function. Another important error is that due to approximating some theoretically computed or measured wave amplitude or pulse by a finite-length time series. Since we are dealing with an infinite-line Cauchy problem, the pulse is assumed to vanish rapidly as $|x| \to \infty$. In the truncation of the signal to a finite length there will always be the possibility of creating "shoulders" at the end of the series where the amplitude abruptly drops to zero. In all results presented in this paper we shall eliminate this source of error by truncating the wave forms only after they have decayed to an amplitude smaller than the selected precision of the input wave. In this way errors of this type do not enter in the present analysis.

5.A. *Cases for One and Two Solitons*

We first consider the one and two soliton solutions of the KdV equation. For these two cases the N-soliton solution reduces to simple formulas which do not require numerical matrix inversion (see the Appendix). These solutions to the KdV equation are therefore very precise and allow closer scrutiny of the errors than does

values of the discrete eigenvalues and of the phase shifts obtained by the DST program for the five cases. For the worst resolution ($\Delta x = 5.0$ cm) the error on the soliton amplitude was less than 1% and for the best resolution the eigenvalue is computed to five decimal places. Note also that the values of the phase shifts are always much smaller than Δx.

Figure 9a shows the two-soliton case; we consider the same five values for Δx considered before. The solitons have amplitude $\eta_1 = 8.0$ cm and $\eta_2 = 6.0$ cm and the input phase shifts are taken to be zero. The continuous curve corresponds to the exact solution and the piecewise continuous curve corresponds again to the worst resolution case $\Delta x = 5.0$ cm. Figure 9b reports the DST spectra for the five cases considered. Again the level of the (spurious) continuous spectrum is rapidly decreasing with Δx. Table III reports the soliton amplitudes and the phase shifts for the five values of Δx considered. Again one observes very small errors for the soliton amplitudes and values of the phase shifts which are much smaller than Δx.

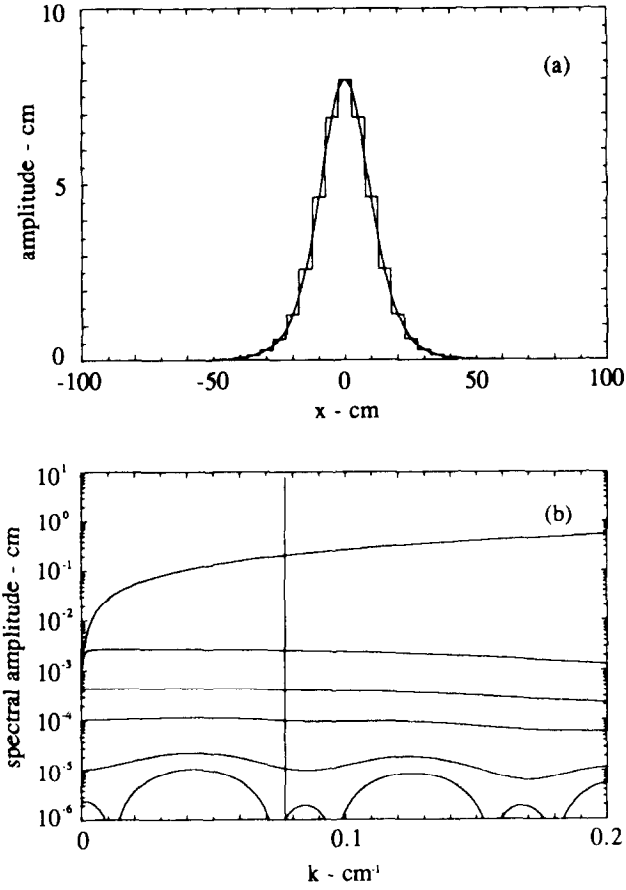

FIG. 8. Single soliton solution of the KdV equation (a) and corresponding DST spectra (b). Both the exact solution and the discretized, piecewise constant wave for a discretization step $\Delta x = 5$ cm are reported in (a). In (b) the upper curve is the saturation spectrum and the other five curves (top to bottom) represent the continuous DST spectra for decreasing values of Δx ($= 5.0$, 2.0, 1.0, 0.4, and 0.2 cm). The vertical line represent the discrete soliton eigenvalue.

TABLE II

Discrete (Soliton) Eigenvalues and Phase Shifts Computed by the DST Algorithm for a Single Soliton Solution with Different Values of the Discretization Step Δx.

Δx (cm)	η_1 (cm)	x_1 (cm)
5.0	7.94755	0.043038
2.0	7.99149	0.006765
1.0	7.99787	0.001606
0.4	7.99966	0.000166
0.2	7.99991	0.000040
exact	8.0	0.0

Note. The last represents the exact results.

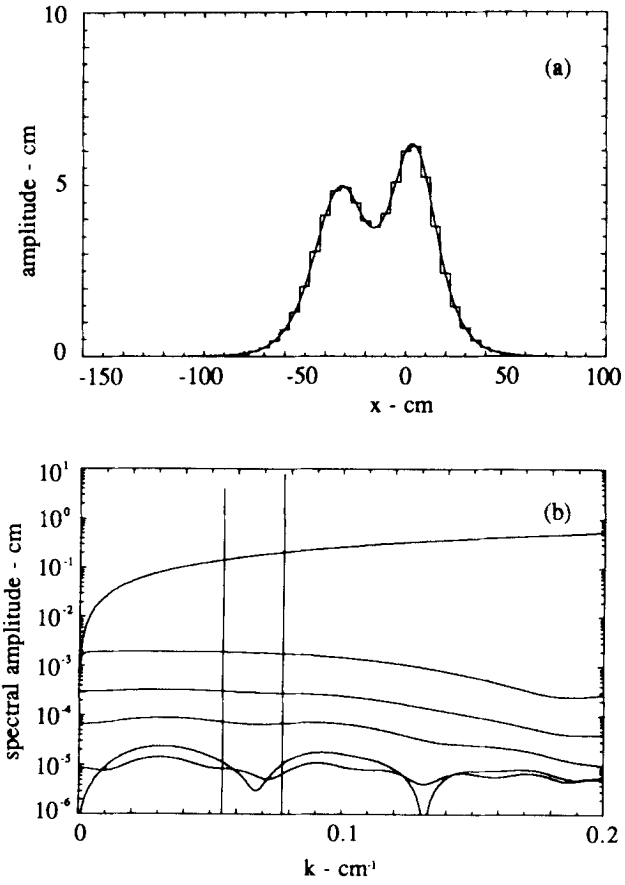

FIG 9. Two-soliton solution of the KdV equation (a) and corresponding DST spectra for different values of the discretization interval (b). Same details as in Fig. 8.

TABLE III

Discrete (Soliton) Eigenvalues and Phase Shifts Computed by the DST Algorithm for a Two-Soliton Solution with Different Values of the Discretization Step Δx

Δx (cm)	η_1 (cm)	x_1 (cm)	η_2 (cm)	x_2 (cm)
5.0	7.98719	-0.008197	3.98256	0.095050
2.0	7.99793	-0.001655	3.99718	0.014654
1.0	7.99949	-0.000667	3.99930	0.003161
0.4	7.99987	-0.000414	3.99982	0.000295
0.2	7.99992	-0.000383	3.99989	-0.000047
exact	8.0	0.0	4.0	0.0

Note. The last represents the exact results.

5.B. *Cases for N Solitons*

We now consider two cases with a larger number of solitons, for which the numerical implementation of the N-soliton (matrix inversion) algorithm is required. The first case is a pure three-soliton wave form which is shown in Fig. 10a together with the discretized wave for $\Delta x = 5$ cm. The soliton amplitudes are $\eta_1 = 8$ cm, $\eta_2 = 6$ cm, and $\eta_3 = 4$ cm. We have selected a zero phase shift for each soliton. Figure 10b reports the DST spectra obtained for the five cases $\Delta x = 5$ cm, 2 cm, 1 cm, 0.4 cm, and 0.2 cm. The continuous DST spectrum is rapidly and monotonically decreasing as Δx decreases. Table IV reports the amplitudes and phase shifts computed by the DST algorithm for the different values of Δx. Note again that the soliton amplitudes are computed with a small error, even with a very coarse discretization step, and that the phase shifts are always much smaller than Δx.

The next case considered is for a pure six-soliton solution of the KdV equation. This wave form and the discretized version with $\Delta x = 5$ cm are shown in Fig. 11a. The soliton amplitudes have been selected to be $\eta_1 = 8$ cm, $\eta_2 = 7$ cm, $\eta_3 = 6$ cm, $\eta_4 = 5$ cm, $\eta_5 = 4$ cm, and $\eta_6 = 3$ cm. The input phase shifts of the solitons have been fixed to be zero. Figure 11b reports the five DST spectra for the values of Δx previously considered. Note that for $\Delta x = 5$ cm a seventh spurious soliton with a rather small amplitude is present in the DST spectrum. The amplitude of this eigenvalue is less than 10^{-3} cm and occurs because of the coarseness of the discretization step. For $\Delta x < 5$ cm this spurious soliton is absent. Table V reports the soliton amplitudes and phase shifts computed by the DST algorithm.

6. Investigation of Random Noise Errors

In this section we consider the DST spectra of signals obtained by superposing a random noise signal on a known wave form. The spectra of the noiseless wave and of the noise itself are assumed known, and we want to determine (a) how the DST spectrum of the noisy wave is modified from that of the noiseless wave form

TABLE IV
Discrete (Soliton) Eigenvalues and Phase Shifts
Computed by the DST Algorithm for a Three-Soliton
Solution with Different Values of the Discretization Step Δx

Δx (cm)	η_1 (cm)	x_1 (cm)	η_2 (cm)	x_2 (cm)	η_3 (cm)	x_3 (cm)
5.0	7.98989	-0.026109	5.98571	0.016600	3.97594	0.100626
2.0	7.99835	-0.004241	5.99768	0.002631	3.99611	0.016136
1.0	7.99959	-0.001064	5.99942	0.000656	3.99903	0.004033
0.4	7.99993	-0.000171	5.99991	0.000103	3.99984	0.000643
0.2	7.99998	-0.000044	5.99998	0.000024	3.99996	0.000159
exact	8.0	0.0	6.0	0.0	4.0	0.0

Note. The last represents the exact results.

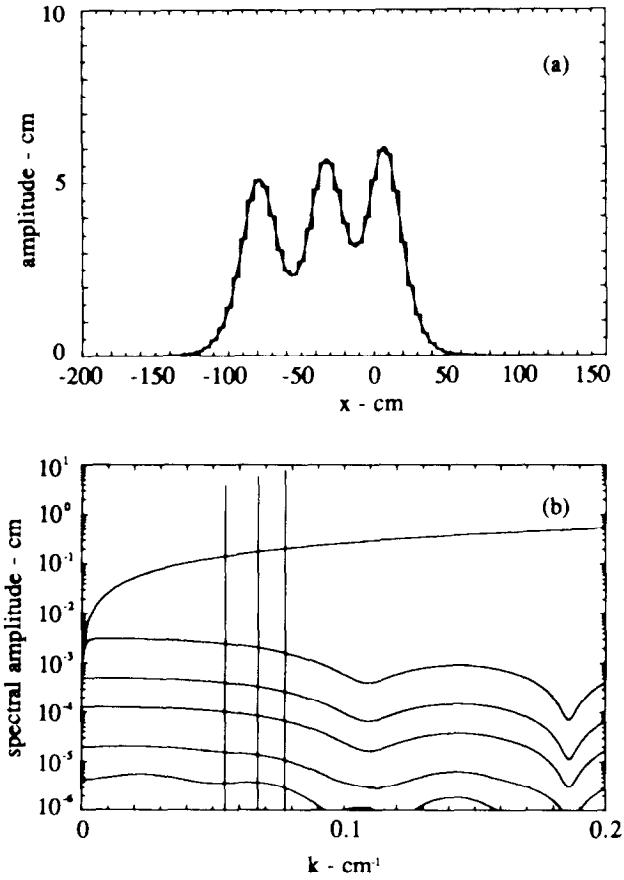

FIG. 10. Three-soliton solution of the KdV equation (a) and corresponding DST spectra for different values of the discretization interval (b). Same details as in Fig. 8.

and (b) how the changes in the spectrum may be characterized. If the problem were linear, the total spectrum would be a simple superposition of the two spectra; this appealing feature is no longer true in general for nonlinear problems. Nevertheless we find that for a wide range of noise amplitudes an approximate spectral superposition is true in an average sense over much of the wavenumber range of the nonlinear DST spectrum as well.

To elucidate this behavior we now consider a pure three-soliton wave form $\eta(x, t)$ on which we linearly superpose random white noise. The noiseless wave form is the three-soliton wave which has already been considered in the previous section; the characteristics of the three solitons are reported in Table VI. We have computed the three-soliton wave form at time $t = 0$ on the interval $-300\text{ cm} < x < 200\text{ cm}$, with discretization interval $\Delta x = 1.0\text{ cm}$. We thus obtain a space series composed of 500 points and length $L = 500\text{ cm}$.

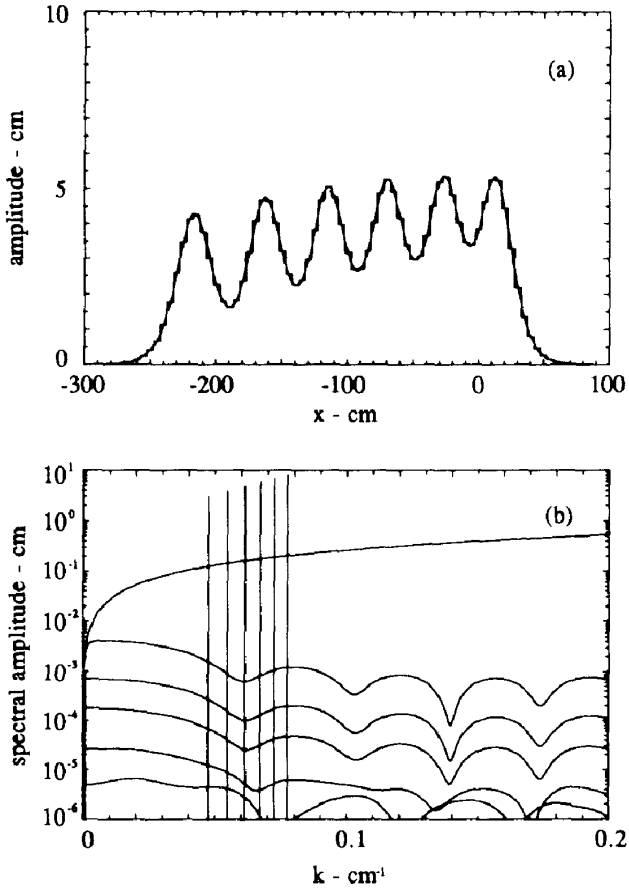

FIG. 11. Six-soluton solution of the KdV equation (a) and corresponding DST spectra for different values of the discretization interval (b). Same details as in Fig. 8.

TABLE V

Discrete (Soliton) Eigenvalues (a) and Phase Shifts

(a) Δx (cm)	η_1 (cm)	η_2 (cm)	η_3 (cm)	η_4 (cm)	η_5 (cm)	η_6 (cm)
5.0	7.99472	6.99346	5.99217	4.99032	3.98694	2.97954
2.0	7.99913	6.99893	5.99870	4.99839	3.99788	2.99670
1.0	7.99978	6.99973	5.99965	4.99956	3.99946	2.99918
0.4	7.99997	6.99995	5.99992	4.99989	3.99991	2.99987
0.2	7.99999	6.99999	5.99996	4.99994	3.99997	2.99997
exact	8.0	7.0	6.0	5.0	4.0	3.0

(b) Δx (cm)	x_1 (cm)	x_2 (cm)	x_3 (cm)	x_4 (cm)	x_5 (cm)	x_6 (cm)
5.0	-0.027812	-0.015927	-0.000397	0.018854	0.049163	0.096125
2.0	-0.004502	-0.002551	0.000108	0.002880	0.007493	0.015443
1.0	-0.001135	-0.000598	0.000217	0.000636	0.001545	0.003912
0.4	-0.000190	-0.000050	0.000257	-0.000001	-0.000140	0.000707
0.2	-0.000055	0.000028	0.000260	-0.000079	-0.000370	0.000224
exact	0.0	0.0	0.0	0.0	0.0	0.0

Note. The last line in each panel represents the exact results.

The noise signal $n(x, 0)$ is random white noise obtained by

$$n(x, 0) = \sum_{j=1}^{J} C_j \cos(k_j x - \phi_j) \tag{6.1}$$

for $-300\text{ cm} \leqslant x \leqslant 200\text{ cm}$, such that again $L = 500$ cm. Note that in writing (6.1)

TABLE VI

Discrete (Soliton) Eigenvalues (a) and Phase Shifts
(b) Computed by the DST Algorithm for a
Three-Soliton Solution with Discretization Step $\Delta x = 0.2$ cm
Contaminated by White Noise with Standard Deviation σ

(a) σ (cm)	η_1 (cm)	η_2 (cm)	η_3 (cm)	η_4 (cm)
0.0	8.0	6.0	4.0	-
0.1	7.99238	6.00231	3.99730	-
0.5	7.96315	6.01205	3.98596	0.00147
1.0	8.05657	5.98644	4.00253	0.00319
3.0	7.87175	6.10650	4.07980	0.07539

(b) σ (cm)	x_1 (cm)	x_2 (cm)	x_3 (cm)	x_4 (cm)
0.0	0.0	0.0	0.0	-
0.1	0.028935	-0.113102	-0.051125	-
0.5	0.145547	-0.568520	-0.256233	-605.600
1.0	0.070502	0.556035	-0.694561	-688.742
3.0	5.607577	3.299054	3.992897	101.848

Note. The first line in each panel represents the exact results in the absence of noise.

we have chosen $t=0$. The signal is discretized into 501 points ($J=501$) with $\Delta x=1.0$ cm. Here $k_j=j\Delta k$, where $\Delta k=2\pi/L$ and the phases ϕ_j are uniformly distributed random numbers between 0 and 2π. For random white noise

$$\begin{aligned} C_j &= C=\text{const}, \qquad k_j \leqslant k_{\max} \\ C_j &= 0, \qquad\qquad k_j > k_{\max}, \end{aligned} \tag{6.2}$$

where $k_{\max}=\pi/\Delta x$. The variance of the signal (6.1) is given by

$$\sigma^2=\sum_{j=1}^{J} C_j^2=JC^2. \tag{6.3}$$

In Fig. 12a we show one realization of formula (6.1) for $\sigma=0.1$ cm. The signal is assumed to lie on the infinite interval $-\infty<x<\infty$, while being identically zero outside the interval $-300\text{ cm}<x<200\text{ cm}$. Figure 12b reports the DST spectrum and the Fourier spectrum of the pure noise of Fig. 12a; these spectra are graphically identical (due to the small wave amplitude used) and are given by the lower solid curve. The upper solid curve is the saturation level discussed in previous sections. The spectra have been graphed with the same scaling used previously.

In Fig. 12b we also graph a horizontal dotted line representing the level given by C and a number of vertical solid lines corresponding to the discrete Fourier amplitudes C_j, each located at $k_j=j\Delta k$. We note that formula (6.1) is valid for a periodic signal, while here instead we study the infinite-line problem. This infinite-line representation of the noise causes changes in the Fourier spectrum of $n(x,0)$, namely: (a) the spectrum becomes continuous since the wavenumber resolution tends to zero; and (b) the spectrum extends to infinity beyond $k_{\max}$. This continuous spectral representation of the noise is given by the continuous line in Fig. 12b.

We also note the importance of scaling the linear, infinite-line transform $|F(k)|$ by $2/L$: with this scaling $F(k)$ is equal, for the wavenumbers given by $k_j=2\pi j/L$, to the discrete Fourier amplitudes C_j of formula (1), as is shown in Fig. 12b. Here we have picked $C_j=C=\text{const}$, and the continuous Fourier spectrum of the pure noise oscillates around the level given by C, which is thus a good measure of the intensity of the noise even in this infinite line problem.

The first example we consider in our analysis of noise effects is for $\sigma=0.1$ cm. The wave field $w(x,0)=\eta(x,0)+n(x,0)$ for this case is shown in Fig. 13a. In Fig. 13b we report the spectrum for $w(x,0)$. The top solid curve is the saturation curve (defined by $b(k)=1$), the middle solid curve is the DST continuous spectrum of $w(x,0)$ and the bottom solid curve is the continuous DST for the discretized wave form $\eta(x,0)$ (since $\eta(x,0)$ contains only solitons this spectral contribution constitutes only the numerical noise). This last curve represents the discretization errors (due to the characteristics of the algorithm itself) as discussed in Section 5. The dashed curve represents the Fourier transform of the pure noise $n(x,0)$. The dotted horizontal line is the level given by C. The discrete DST spectrum is

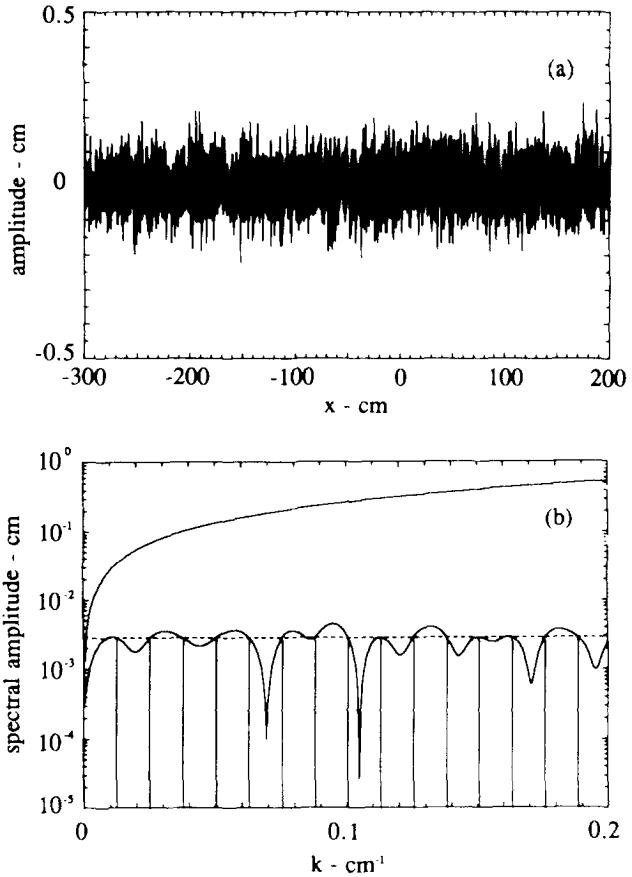

FIG. 12. Pure white noise with $\sigma = 0.1$ cm (a) and corresponding DST spectrum (b). The horizontal dashed line represents the level of the white noise (the constant C in Eq. (6.1)) and the vertical solid lines represent the Fourier spectral amplitudes used in the generation of the white noise signal (Eq. (6.1)).

composed of three solitons as indicated by the arrows. The relevant quantities for these solitons are given in Table VI.

As one can see the (noise-generated) continuous DST spectrum of $w(x, 0)$ is very similar to the Fourier spectrum of the pure noise. The DST spectrum of $w(x, 0)$ is, practically speaking, the superposition of the spectra for $\eta(x, 0)$ and $n(x, 0)$ and the value of C gives a very good measure of the level of the continuous DST spectrum of $w(x, 0)$. The discrete eigenvalues (the solitons) are changed only slightly by the presence of noise.

In Fig. 13c we give the wave form obtained by taking the inverse spectral transform of the discrete part of the spectrum of $w(x, 0)$ (solid line) and the original wave form $\eta(x, 0)$ (dashed line). The two curves coincide to within graphical precision: the noise has almost no effect on the recognition of the correct

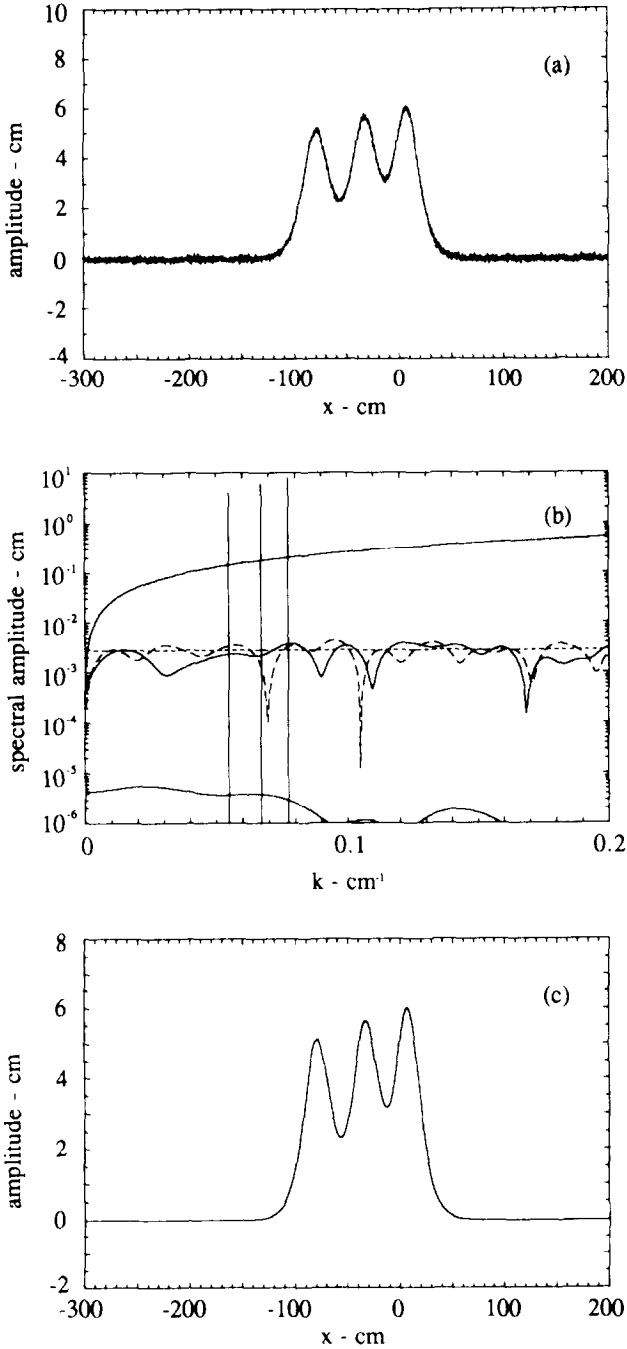

FIG. 13. Three-Soliton wave form with superposed random white noise with $\sigma = 0.1$ cm (a), corresponding DST spectrum (b), and reconstructed pure soliton solution (c). In (b) the upper solid curve is the saturation spectrum, the intermediate solid curve is the continuous DST spectrum of the wave in Fig. 13a, the lower solid curve is the spurious continuous spectrum generated by the discretization procedure, the long dashed curve is the Fourier spectrum of pure noise and the horizontal short-dashed line is the level given by C (Eq. (6.3)). The vertical lines represent the soliton eigenvalues. In (c) both the reconstructed wave (solid line) and the exact three-soliton solution (dashed line) are drawn. In this case the two curves are indistinguishable.

characteristics of the solitons. We note that the inversion of the discrete soliton spectrum constitutes nonlinear filtering of the noise. This important point is discussed further below.

In Fig. 14a we show the wave form $w(x, 0)$ for the three-soliton case plus random white noise with standard deviation $\sigma = 0.5$ cm. The noise is now rather intense. The spectrum of $w(x, 0)$ is shown in Fig. 14b. Again the continuous DST spectrum is very similar to the Fourier spectrum of the pure noise $n(x, 0)$ and its level is very well characterized by C. The simple superposition of the spectra of $\eta(x, 0)$ and $n(x, 0)$ is slightly broken by the appearance of a very small discrete eigenvalue added to the original three. The characteristics of the solitons for this case are reported in Table VI in Fig. 14c we show (solid line) the wave form obtained by inverting the discrete part of the spectrum presented in Fig. 14b (nonlinearly filtering out the noise), compared to the original wave $\eta(x, 0)$ (dashed line). The differences between the two curves (barely within graphical precision) are mainly due to a small phase shift of the solitons, introduced by the presence of the noise.

We note here that if we consider the added random noise as a model for experimental errors present in a measured wave signal, the two cases presented above are the significant ones. Noise more intense than the above is (hopefully) hardly ever found in experimental data. Thus, the two cases we now discuss are considered to be extreme examples of the ability of the DST algorithm for finding the important nonlinear characteristics of a signal, even when they are deeply hidden in very intense noise. Figure 15a shows a case with $\sigma = 1.0$ cm. The original wave form is quite obscured by the noise. The spectrum for this case is shown in Fig. 15b. The continuous DST spectrum and the Fourier spectrum are very similar; here a sort of superposition holds and C gives a good measure of the level of the continuous DST spectrum (due entirely to the noise) for $n(x, 0)$. A fourth spurious soliton with low amplitude is present in the DST spectrum. In Fig. 15c we show the reconstruction of the signal associated with the discrete DST spectrum (solid line) and the original wave $\eta(x, 0)$. The presence of the fourth soliton is not very evident and the two curves differ only slightly, mainly by the phase shifts of the reconstructed solitons. Again see Table VI for a collection of the characteristics of the discrete DST spectrum for this case. The power of nonlinear spectral analysis based on the DST algorithm is clearly evident at this point: even if the solitons are almost completely obscured by the noise as in Fig. 15a, the DST spectrum furnishes a clear interpretation of the components.

The last case considered is shown in Fig. 16a (note the change of the vertical scale). Here $\sigma = 3.0$ cm. The original wave is almost completely erased by the noise. The spectrum is reported in Fig. 16b. One can clearly see the saturation of the continuous DST for $k < 0.2$ cm^{-1}, and the related increase in amplitude and wave number of the forth spurious soliton. We filter out the noise by inverting the discrete DST spectrum to give the signal in Fig. 16c (solid curve) compared to $\eta(x, 0)$ (dashed curve). The fourth soliton is now evident, but again the three original solitons are only slightly changed and phase shifted. For this case as well the relevant parameters for the discrete eigenvalues are collected in Table VI.

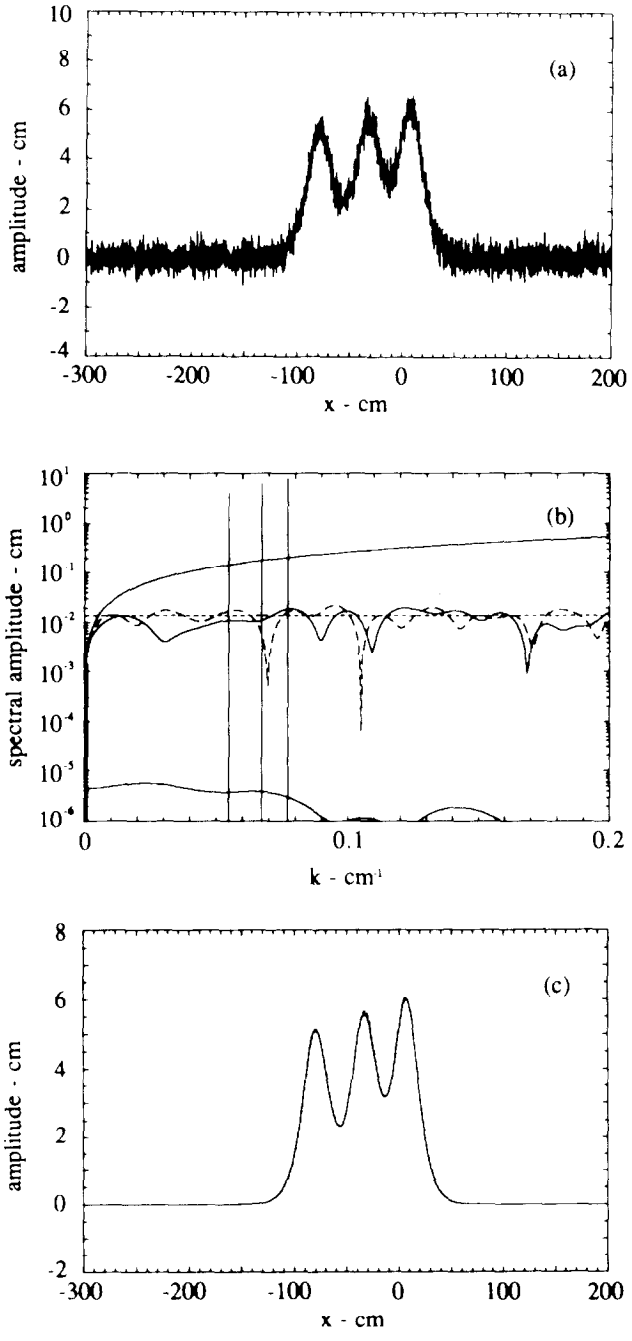

FIG. 14. Three-soliton wave form with superposed random white noise with $\sigma = 0.5$ cm (a), corresponding DST spectrum (b), and reconstructed pure soliton solution (c). Same details as in Fig. 13.

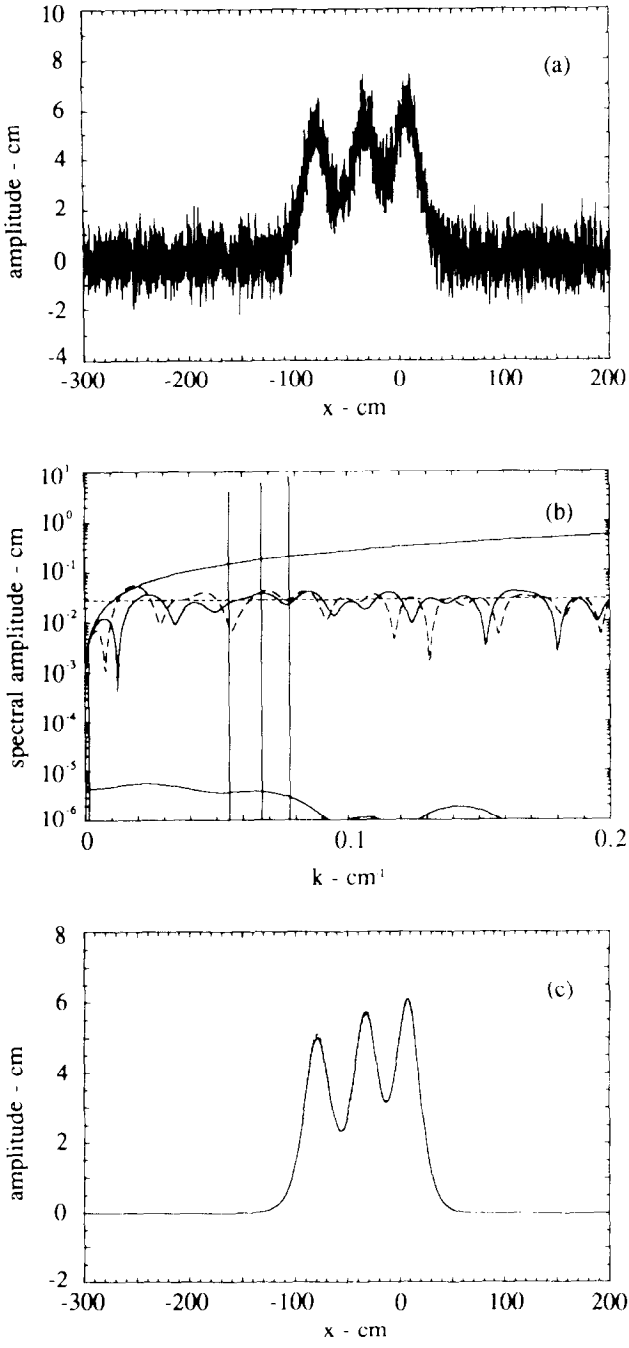

FIG. 15. Three-soliton wave form with superposed random white noise with $\sigma = 1.0$ cm (a), corresponding DST spectrum (b), and reconstructed pure soliton solution (c). Same details as in Fig. 13.

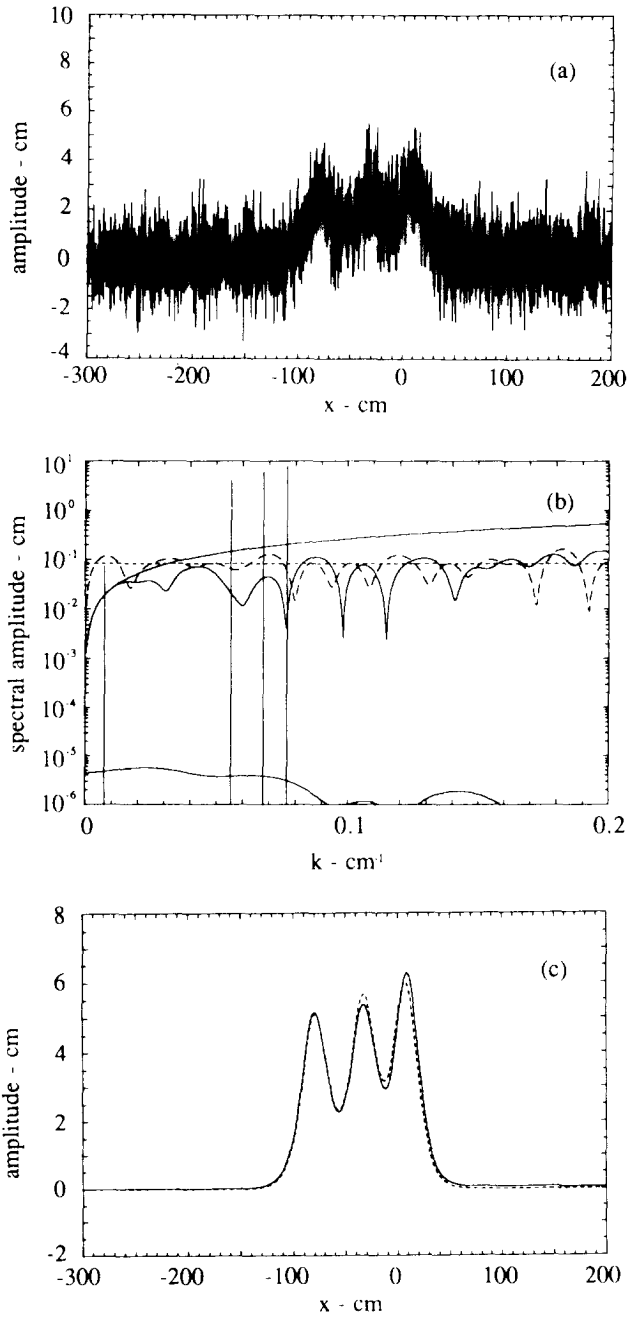

FIG. 16. Three-soliton wave form with superposed random white noise with $\sigma = 3.0$ cm (a), corresponding DST spectrum (b), and reconstructed pure soliton solutin (c). Same details as in Fig. 13.

The conclusions of the above analysis of three interacting solitons plus noise may be summarized as follows:

(a) For noise amplitudes not too great (not obscuring the original wave form) the continuous DST spectrum is very similar, on the average, to the Fourier spectrum of the pure noise. The level of the continuous spectrum is approximately characterized by the constant Fourier amplitude C.

(b) For low noise levels an approximate superposition between the original wave and the noise holds, even in the presence of nonlinear effects. The above analysis was conducted considering an original wave form with a purely discrete DST spectrum (e.g., only solitons). For a more general wave form, in which both solitons and radiation coexist, the continuous spectrum is a near superposition of the noiseless continuous spectrum and of the noise spectrum (except, possibly, at very low wavenumbers, where saturation and generation of low amplitude, spurious discrete eigenvalues may take place).

(c) For large noise amplitudes spectral superposition holds for high wavenumbers, but at low wavenumbers the continuous DST spectrum becomes saturated (i.e., $b(k) = 1$). Part of the noise energy at low wavenumbers contributes to generation of a spurious (false) soliton whose wavenumber and amplitude increase with the noise intensity.

(d) The discrete DST spectrum of the original wave remains robust for reasonable noise intensities. The amplitudes of the solitons are not disturbed very much, and the changes in amplitude are much less than the r.m.s. of the noise. There is also the possibility of a phase shift of the solitons due to the presence of the noise. The spurious soliton always has an amplitude less than the r.m.s. of the noise, and its wavenumber (and thus its amplitude) is probably related to the extent of the saturated region in the continuous DST spectrum.

The results of this section indicate that the DST algorithm provides a rigorous tool for the nonlinear filtering of signals described by the KdV equation. While a linear filter would be unable to recover the soliton component from the noise background, use of the DST approach furnishes a nonlinear spectrum in which the soliton and the noise components are well defined and may, therefore, be treated separately. If one is interested in the soliton component, for example, then the knowledge of the soliton amplitudes and phases (provided by the DST spectrum) and their use in an N-soliton algorithm allows a pure N-soliton wave form to be extracted from the noise. In the analysis above we have precisely followed this route and we have reconstructed the soliton signal originally obscured by noise. We expect nonlinear filtering to be important in the analysis of experimental data.

7. Summary and Conclusions

In this paper we have applied the numerical DST algorithm developed in the companion paper (I) to a number of example problems in order to test for

numerical precision. Roundoff errors have been analyzed by considering the DST spectra of positive and negative square input wave forms. The DST spectra for these waves can be computed exactly, allowing a comparison of theoretical and numerically computed spectra, and the DST algorithm was found to be influenced very little (and in a quite predictable way) by roundoff errors. Another important result is that the errors on the soliton amplitudes computed by the numerical DST are always of the order of the uncertainty on the input wave form; i.e., the input precision is essentially maintained by the algorithm and consequently the input errors are not amplified by nonlinear effects.

We have also considered the errors introduced by discretization of the input wave form. To evaluate discretization errors we have considered a pure N-soliton solution for which the continuous spectrum is theoretically absent. As a result of the discretization a (spurious, small amplitude) continuous spectrum is produced. This allows for careful estimates to be made of the errors in the DST spectrum as a function of the discretization step.

Since we are primarly interested in the application of the DST algorithm to experimental data we have also considered how the DST spectra are modified by the presence of random noise. To this end we have selected a pure three-soliton wave form and superposed a white noise signal on it. For noise amplitudes which do not completely mask the original wave form the DST spectra are the quasi-linear superposition of a discrete spectrum corresponding to the solitons and of a continuous spectrum which is, on the average, near the level of the noise intensity. For very low wavenumbers this superposition does not hold (since the continuous spectrum is saturated here), and additional spurious solitons can be generated by the presence of the noice. The amplitudes of these solitons is, however, always smaller than the noise intensity, and the original solitons are correctly identified, both in amplitude and phase, by the DST algorithm. For large noise amplitudes, such that the original wave form is almost masked by the noise, the solitons are still correctly identified. In this case, however, an energetic continuous spectrum and spurious solitons (always of amplitude smaller than the noise) are present. These extreme cases indicate that the DST algorithm may be successfully employed for extracting the soliton component from a strong background noise signal. This analysis also suggests that the DST approach can be used for the nonlinear filtering of signals described by the KdV equation. We hope that these results may provide a stimulus for the future use of nonlinear spectral analysis methods in the study of nonlinear phenomena.

Appendix: Algorithm for the N-Soliton Solution

The exact N soliton solution of the KdV equation (Segur [30], Whitham [31], and cited references) is found when the radiation spectrum is identically zero, $b(k)=0$. In this case the DST spectrum is given by

$$\mathrm{DST} = \{K_n, C_n, N, 1 \leqslant n \leqslant N; b(k)=0\}. \tag{A.1}$$

Explicitly the wave amplitude as a function of space x and time t is given by

$$\eta(x, t) = (2/\lambda) \frac{d[\mathrm{Tr}(\mathbf{P}^{-1}\, d\mathbf{P}/dx]}{dx} \tag{A.2}$$

or equivalently by

$$\eta(x, t) = (2/\lambda) \frac{d^2 \ln[\det \mathbf{P}]}{dx^2}. \tag{A.3}$$

Here Tr $\mathbf{P}$ denotes the trace of $\mathbf{P}$, det $\mathbf{P}$ is the determinant of $\mathbf{P}$, and $\lambda = \alpha/6\beta$, see Eq. (2.1). The matrix $\mathbf{P}$ is of dimension N with elements P_{ij} given by

$$P_{ij} = \delta_{ij} + \frac{C_i C_j}{(K_i + K_j)} e^{[-(K_i + K_j)x + (\Omega_i + \Omega_j)t]}, \tag{A.4}$$

where δ_{ij} is the Kronecker delta and $i, j = 1, 2, ..., N$. Here K_n, C_n are the eigenwavenumbers and phase coefficients defined in the text. The eigenfrequencies Ω_i are given by

For the numerical implementation of the N-soliton solution we note that (A.3) requires the numerical evaluation of a double derivative, a procedure which can lead to a compromise in accuracy. To alleviate the problem we use (A.2) instead and rewrite it as

$$\begin{aligned} \eta(x, t) &= (2/\lambda)\, \mathrm{Tr}\left(\frac{d(\mathbf{P}^{-1}\, d\mathbf{P}/dx)}{dx}\right) \\ &= (2/\lambda)\, \mathrm{Tr}\left(-\mathbf{P}^{-1}\frac{d\mathbf{P}}{dx}\,\mathbf{P}^{-1}\frac{d\mathbf{P}}{dx} + \mathbf{P}^{-1}\frac{d^2\mathbf{P}}{dx^2}\right). \end{aligned} \tag{A.6}$$

Explicit expressions are obtainable for the elements of $d\mathbf{P}/dx$ and $d^2\mathbf{P}/dx^2$; this eliminates the need for numerical derivatives. It has also proven useful to redefine $\mathbf{P}$ by using the property that the wave field $\eta(x, t)$ is unchanged if each element of $\mathbf{P}$ is multiplied by the expression $\exp(K_i\, \Delta x)$. We thus write

$$P_{ij} = e^{[(K_i + K_j)x \quad (\Omega_i + \Omega_j)t]} + \frac{C_i C_j}{(K_i + K_j)} \tag{A.7}$$

$$\left(\frac{d\mathbf{P}}{dx}\right)_{ij} = (K_i + K_j)\, e^{[(K_i + K_j)x - (\Omega_i + \Omega_j)t]} \tag{A.8}$$

$$\left(\frac{d^2\mathbf{P}}{dx^2}\right)_{ij} = (K_i + K_j)^2\, e^{[(K_i + K_j)x - (\Omega_i + \Omega_j)t]}. \tag{A.9}$$

With the definition (A.7) for $\mathbf{P}$, the matrices $d\mathbf{P}/dx$ and $d^2\mathbf{P}/dx^2$ are diagonal.

The remaining numerical operation is the inversion of **P**. However, det **P** is small for large negative values of x and large values of N. Using double precision arithmetic we have found good results up to about 10 solitons.

In the case of a single-soliton or of a two-soliton solution of the KdV equation the N-soliton solution reduces to a simple analytical expression and no numerical inversion of **P** is required. For the single soliton,

$$\eta(x, t) = \eta_1 \operatorname{sech}^2(K_1(x - x_1) - \Omega_1 t), \tag{A.10}$$

where η_1 is the soliton amplitude which is related to the soliton wavenumber K_1 by the formula

$$\eta_1 = \frac{2K_1^2}{\lambda} \tag{A.11}$$

and the phase shift x_1 is given by

$$x_1 = \frac{1}{2K_1} \ln\left(\frac{C_1^2}{2K_1}\right), \tag{A.12}$$

where C_1 is the normalization coefficient of the (single) eigenfunction corresponding to the eigenwavenumber K_1 and is defined in the text.

In the two-soliton case the formula is written as

$$\eta(x, t) = \left[8K_1^2 \left\{ f_2^{-1} + \left(\frac{K_1 - K_2}{K_1 + K_2}\right) f_2 \right\}^2 + 8K_2^2 \left\{ f_1^{-1} + \left(\frac{K_2 - K_1}{K_2 + K_1}\right) f_1 \right\}^2 \right] \times \left[\left\{ \frac{1}{f_1 f_2} + \frac{f_1}{f_2} + \frac{f_2}{f_1} + \left(\frac{K_1 - K_2}{K_1 + K_2}\right)^2 f_1 f_2 \right\}^2 \right]^{-1}, \tag{A.13}$$

where

$$f_j = C_j \exp[K_j(x - x_j) - \Omega_j t]; \qquad j = 1, 2, \tag{A.14}$$

and K_1 and K_2 are the wavenumbers of the two solitons, Ω_1 and Ω_2 their frequencies, C_1 and C_2 are the normalization coefficients, and x_1 and x_2 are the soliton phase shifts which are given by (A.12) (interchange the subscripts for the second soliton).

ACKNOWLEDGMENTS

We acknowledge the continuing encouragement of Professors L. Bergamasco and C. Castagnoli of the University of Torino, Italy, without whose support this work could not have been done.

REFERENCES

1. M. J. ABLOWITZ AND H. SEGUR, *Solitons and the Inverse Scattering Transform* (SIAM, Philadelphia, 1981).
2. C. S. GARDNER, J. M. GREENE, M. D. KRUSKAL, AND R. M. MIURA, *Phys. Rev. Lett.* **19**, 1095 (1967).
3. G. L. LAMB, *Elements of Soliton Theory* (Wiley, New York, 1980).
4. V. E. ZAKHAROV, S. V. MANAKOV, S. P. NOVIKOV, AND L. P. PITAYEVSKY, *Theory of solitons. The Method of the Inverse Scattering Problem* (Nauka, Moscow, 1980). [Russian]
5. F. CALOGERO AND A. DEGASPERIS, *Spectral Transform and Solitons: Tools to Solve and Investigate Nonlinear Evolution Equations. Volume I* (North-Holland, Amsterdam, 1982).
6. R. K. DODD, J. C. EILBECK, J. D. GIBBON, AND H. C. MORRIS, *Solitons and Nonlinear Wave Equations* (Academic Press, London, 1982).
7. M. J. ABLOWITZ AND J. LADIK, *J. Math. Phys.* **16**, 598 (1975); *J. Math. Phys.* **17**, 1011 (1976); *Stud. Appl. Math.* **55**, 213 (1976); *Stud. Appl. Math.* **57**, 1 (1977).
8. A. R. OSBORNE, *J. Comput. Phys.* **94**, 284 (1991).
9. A. R. OSBORNE, A. PROVENZALE, AND L. BERGAMASCO, *Nuovo Cimento C* **5**, 597 (1982).
10. A. R. OSBORNE, A. PROVENZALE, AND L. BERGAMASCO, *Nuovo Cimento C* **5**, 612 (1982).
11. A. R. OSBORNE, A. PROVENZALE, AND L. BERGAMASCO, *Nuovo Cimento C* **5**, 633 (1982).
12. A. R. OSBORNE, A. PROVENZALE, AND L. BERGAMASCO, *Nuovo Cimento Lett.* **36**, 593 (1983).
13. A. R. OSBORNE, in *Statics and Dynamics of Nonlinear Systems, Proc. of a Workshop at the Ettore Majorana Centre*, edited by G. Benedek, H. Bilz, and R. Zeyher (Springer-Verlag, New York/Berlin, 1983).
14. A. R. OSBORNE, M. PETTI, G. LIBERATORE, AND L. CAVALERI, in *Computer Modelling in Ocean Engineering*, edited by B. A. Schrefler and O. C. Zienkiewicz (Balkema, Rotterdam, 1988).
15. A. R. OSBORNE, in *Soliton Theory: A Survey of Results*, edited by A. P. Fordy (Manchester Univ. Press, Manchester, UK, 1990).
16. A. R. OSBORNE, in *Nonlinear Topics in Ocean Physics, Proc. of the Int. School of Physics "E. Fermi,"* edited by A. R. Osborne (Elsevier, Amsterdam, 1991).
17. A. R. OSBORNE AND L. BERGAMASCO, *Nuovo Cimento B* **85**, 229 (1985).
18. A. R. OSBORNE AND L. BERGAMASCO, *Physica D* **18**, 26 (1986).
19. D. J. BENNEY, *J. Math. Phys.* **45**, 52 (1966).
20. T. MAXWORTHY AND L. G. REDEKOPP, *Nature* **260**, 509 (1976).
21. L. G. REDEKOPP AND P. D. WEIDMAN, *Icarus* **33**, 388 (1978).
22. P. MALANOTTE RIZZOLI AND M. C. HENDERSHOTT, *Dyn. Atmos. Oceans* **4**, 247 (1980).
23. J. P. BOYD, *J. Phys. Oceanogr.* **10**, 1699 (1980).
24. P. MALANOTTE RIZZOLI, "Planetary Solitary Waves," in *Advances in Geophysics* (Academic Press, New York, 1982).
25. V. I. KARPMAN, *Non-linear Waves in Dispersive Media* (Pergamon, Oxford, 1975).
26. A. R. OSBORNE, A. D. KIRWAN, A. PROVENZALE, AND L. BERGAMASCO, *Phys. Fluids* **29**, 656 (1986).
27. H. SEGUR, in *Topics in Ocean Physics, Proc. of the Int. School of Physics "E. Fermi,"* edited by A. R. Osborne and P. Malanotte Rizzoli (North-Holland, Amsterdam, 1982).
28. A. C. NEWELL, *Solitons in Mathematics and Physics* (SIAM, Philadelphia, 1985).
29. A. R. OSBORNE AND G. BOFFETTA, *Phys. Fluids A* **1**, No. 7, 1200 (1989).
30. H. SEGUR, *J. Fluid Mech.* **59**, 721 (1973).
31. G. B. WHITHAM, *Linear and Nonlinear Waves* (Wiley, New York, 1974).